

Magnetohydrostatic atmospheres

Laurence J. November

The Light Physics, La Luz NM 88337-0217 USA

April 28, 2003

Abstract. We show that the atmospheric and magnetic height variations are coupled in all magnetohydrostatic (MHS) equilibria with gravity if any isolated weak evacuated flux tubes or hydrostatically connected non-force-free fields are present. In gas-dominated regimes, as in stellar photospheres, flux tubes expand with height to maintain pressure balance with the ambient giving a ‘magnetic canopy’ in the relatively small-scale-height cool atmosphere. But in magnetically dominated regimes, as in stellar coronae, the lines of the large-scale background magnetic field determine the spreading of embedded flux tubes. There rigidly held flux tubes *require* a specific minimum surrounding atmosphere with a unique temperature profile for equilibrium. The solar static equilibrium atmosphere exhibits the correct transition-region properties and base coronal temperature for the sun’s main magnetic spherical harmonic. Steady flows along field lines may contribute to the overall pressure, so equilibria with accelerated wind outflows are possible as well. Flux tubes *do not play a dynamical role*, but rather indicate a mathematical degeneracy in the form of non-force-free magnetic fields. Equilibria are naturally self restoring and dynamics tend to maintain the MHS atmosphere. Outflows are produced in perturbed equilibria that fill a depleted or cool atmosphere to the equilibrium gas profile, which heats the gas compressively.

Key words. magnetohydrodynamics (MHD) – Sun:magnetic fields – Sun:atmosphere – Sun:corona – Sun:transition region

1. Introduction

In our observation of coronal ‘threads’ (November & Koutchmy, 1996), we puzzled over whether coronal flux tubes should expand with height to maintain pressure balance with the ambient gas-pressure decrease or follow the lines of the external magnetic field. After all, if the atmosphere were independently heated, the gas and magnetic height variations should be generally different. Observations of > 15 Mm ‘voids’ (MacQueen et al., 1974, 1983), > 2 Mm threads, and > 1 km filamentary microstructure (Coles & Harmon, 1978; Woo et al., 1995; Woo & Habbal, 1997) suggest that the large-scale solar coronal magnetic field contains isolated weak embedded flux tubes in a great range of sizes. Figure 1 shows dark and bright threads in a square region about a solar radius on a side over the west limb taken with the Canada-France-Hawaii Telescope (CFHT) at the unique total-eclipse opportunity on Mauna Kea on July 11, 1991. The dark and bright threads, which were essentially unchanged over the 4-minute eclipse duration, appear to be aligned and organized in arched and radial surfaces probably current sheets overlapping in their projection onto the plane of the sky in the line-of-sight view.

We know that isolated flux tubes must expand with height to follow the ambient gas-pressure decrease. The flux-tube gas-

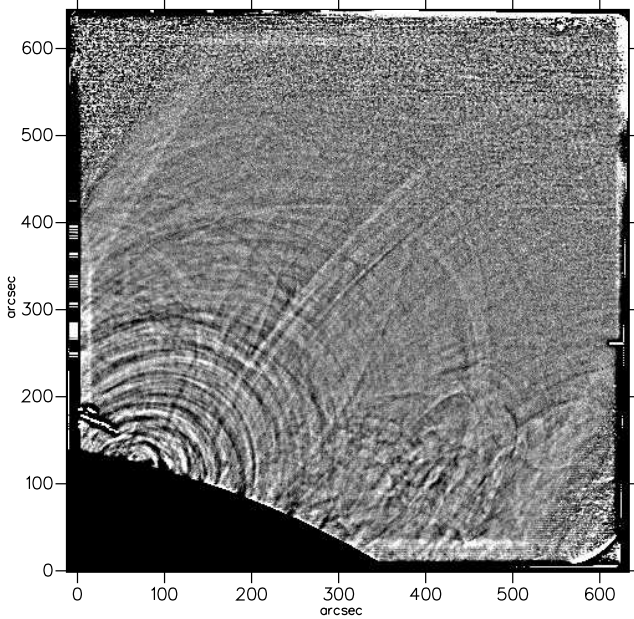


Fig. 1. Unsharp-masked time-averaged white-light eclipse image processed by subtracting a 6 arcsec = 4300 km Gaussian convolution. The full contrast range is $\Delta \ln(I) = \Delta I/I = 0.8\%$. Dark and bright threads appear to be flux tubes in current sheets.

pressure difference, external minus internal, is related to the magnetic-pressure difference by the static equilibrium relation

$$p_e - p_i = \frac{1}{8\pi} (\mathbf{B}_i^2 - \mathbf{B}_e^2). \quad (1)$$

Correspondence to: nov@thelightphysics.org

The Wilson depression in sunspots shows that at least large-scale photospheric flux tubes are nearly evacuated. Evacuated flux tubes exhibit the maximum magnetic concentration and field strength possible. In evacuated flux tubes $p_i = 0$ and the photospheric external ambient $\mathbf{B}_e = 0$, so the internal field strength must follow the ambient gas-pressure decrease, $\mathbf{B}_i(r)^2 = 8\pi p_e(r)$, giving a flux tube that expands with height to conserve its total internal magnetic flux. Since the scale height for $p_e(r)$ is relatively small in the cool photosphere a dramatic flux-tube expansion occurs, which is the accepted explanation for the solar ‘magnetic canopy’ (Giovanelli & Jones, 1982; Giovanelli, 1982). Both voids and a range of sizes of dark threads were also found to have contrasts consistent with what is expected for fully evacuated cylindrical flux tubes. In the corona, where the external magnetic field is not zero, the magnetic flux inside evacuated flux tubes must decrease with height to follow the total external ambient gas plus magnetic pressures, $\mathbf{B}_i(r)^2 = 8\pi p_e(r) + \mathbf{B}_e(r)^2$, giving a small flux-tube expansion with height in the much larger pressure scale height of the hot corona. A slight flux-tube expansion with height seems evident in some of the threads in figure 1.

We can argue too that the radial expansion of isolated flux tubes must follow the external magnetic field. Parker (1972) proved that

$$(\mathbf{B}_e \cdot \nabla) \mathbf{B}_i = 0, \quad (2)$$

in MHS equilibria without gravity, where \mathbf{B}_e represents a uniform background magnetic field and the field in flux tubes \mathbf{B}_i contains all of the spatial variations; by assumption the spatially varying component is relatively small, $|\mathbf{B}_i - \mathbf{B}_e| \ll |\mathbf{B}_e|$. Parker’s theorem is locally applicable everywhere in perturbed MHS equilibria with gravity, i.e. equation (2) with \mathbf{B}_e allowed to vary slowly spatially as we discuss in §2. Thus isolated weak flux tubes in a gravitational field must spread to follow the lines of the background magnetic field; the radial functional variations must be directly related; $|\mathbf{B}_i(r)| \propto |\mathbf{B}_e(r)|$ along flux tubes.

Therefore both ways of looking at the problem are correct. The coronal flux-tube field must follow the external field, $\mathbf{B}_i(r)^2 \propto \mathbf{B}_e(r)^2$, and the radial variation of the external gas pressure outside isolated evacuated coronal flux tubes is proportional to the magnetic-pressure difference, $p_e(r) \propto \mathbf{B}_i(r)^2 - \mathbf{B}_e(r)^2$. Hence the external gas and magnetic pressures must be coupled with $p_e(r) \propto \mathbf{B}_e(r)^2$ outside and along isolated weak evacuated flux tubes. Since the ambient magnetic field is dominant in lower stellar coronae having about 100 times the energy density of the gas, it must be essentially unperturbed and determine the expansion of embedded flux tubes. The expansion of weak evacuated flux tubes then defines the radial variation of the ambient gas pressure for equilibrium, the gas pressure being horizontally stratified in the external force-free or potential field.

The properties of flux tubes reflect a natural degeneracy in the form of non-force-free magnetic fields, and imply the existence of an underlying *mathematical* relationship between the atmospheric and magnetic height variations as described in §2. It is important to realize that we do not suggest that flux tubes play any dynamical heating role. Weak embedded non-force-free magnetic fields in an otherwise force-free field tend to

exist as isolated flux tubes. Flux-tube evacuation occurs with an excess field strength $|\mathbf{B}_i(r)| > |\mathbf{B}_e(r)|$ and *requires* a minimum surrounding atmosphere to exist in equilibrium. A relatively cool nonevacuated flux tube with excess field strength tends to evacuation with height. Otherwise nonevacuated flux tubes should usually be hydrostatically connected to the surrounding force-free field with $p_i(r) \propto p_e(r)$, thereby exhibiting the same external atmosphere with $p_e(r) \propto \mathbf{B}_e(r)^2$ along flux tubes. Thus a mostly force-free atmosphere containing any of the usual forms of weak non-force-free magnetic fields must exhibit an equilibrium radial pressure variation determined by the background magnetic field or a specific temperature profile for a perfect gas in hydrostatic equilibrium.

Historical MHS equilibrium solutions with gravity have suggested that a general mathematical relationship exists between the large magnetic and gas-pressure scales. Dungey (1953) derived plane-parallel MHS equilibria for a magnetic field having its degenerate axis directed perpendicular to gravity (see also Low 1975; Cheng & Choe 1998). The solutions are represented in a modified Grad-Shafranov (GS) Equation, which retains the gas-pressure radial scale-height variation as a separable factor in the pressure term. Dungey showed that when the magnetic field is also zero in its degenerate axis, the separable factor can be absorbed into the coordinates giving the classical GS Equation in a remapped coordinate system. The new GS coordinates are defined by the gas-pressure scale height, meaning that magnetic fields in a prespecified atmosphere must be spatially distorted. Example horizontal magnetic flux tubes can exhibit substantial radial deformation in a solar corona of given constant temperature (Zweibel & Hundhausen, 1982; Low, 1992). Depending upon their size compared to the gas-pressure scale height, flux tubes are either compressed or expanded in the gravitational direction and approximately undistorted only in a specific atmosphere.

In §2, we show that cross-field conditions lead to coupled gas- and magnetic-pressure height variations in general non-force-free MHS equilibria. Steady flows do not alter the coupling but may produce a Bernoulli pressure that contributes to the gas pressure leading to possible accelerated steady wind outflows. In §3, we examine equilibrium radial profiles of temperature and flux-tube diameter using a common scale-height function that correctly represents the height variation of the dominant pressure component, gas or magnetic, in regimes where one component is dominant. The profiles reproduce the salient features of the solar atmosphere: the rapid expansion of flux tubes in the photosphere where the atmospheric gas pressure is dominant, a transition region of proper thickness located just above the height where the gas and magnetic energy densities are equal, and a corona of correct base temperature for the sun’s main magnetic spherical harmonic.

Although the dynamics of the system can be quite complicated exhibiting possible disequilibria, which may take the form of evolving deviations or ongoing small-scale magnetic instabilities, it does seem reasonably accepted that the equilibrium state must characterize the average condition of any system satisfying the ‘quasi-steady’ conditions (Low, 1980). Hot stellar coronae are naturally restored by the hydrodynamics as we discuss in §4.

2. MHS Equilibria with Gravity

The equations for static equilibrium in a gravitational field are Gauss' Law and the MHS equation

$$\mathbf{B} \cdot \mathbf{B} = 0, \quad (3)$$

$$\nabla p + \frac{p}{h} \nabla r = \frac{1}{4\pi} (\nabla \times \mathbf{B}) \times \mathbf{B}. \quad (4)$$

The atmospheric contribution to the pressure scale height is directly related to the temperature for a perfect gas, $h \equiv p/(\rho g(r)) = kT/(\bar{m}g(r))$. The variables have their usual meanings: \mathbf{B} is the magnetic field vector in Gaussian units, \mathbf{J} the current density (used below), \mathbf{u} the flow velocity (used below), p the gas pressure, ρ the density, T the temperature, k Boltzman's constant, \bar{m} the mean particle mass, c the speed of light (used below), and $g(r) = GM_\odot/r^2$ is the gravitational acceleration, with G the universal gravitational constant and M_\odot the stellar mass. The coordinate r measures the distance from the stellar center, and the formal notation ∇r is adopted for algebraic convenience to denote the radially directed unit vector.

The set of four vector-component equations (3 – 4) contain five unknowns, p , h , and the three vector components of \mathbf{B} . However the solution space for \mathbf{B} is more restrictive than would be obtained with linear relations as we discuss in this section and elaborate in Appendix A.

The gravitational term in equation (4) compared to the pressure gradient is of order d/h , where d is a characteristic flux-tube thickness; for the main power in threads in the solar corona $d/h < 10^{-3}$. The equation is the same as the unperturbed MHS equation (A.1) except that $\nabla p \rightarrow (\nabla + \nabla r/h)p$, indicating that the pressure gradient is slightly modified in the presence of a gravitational field. In the vicinity of non-force-free fields, gas-pressure changes must be mainly magnetically determined, and only far away can the gravitational gradient be significant. Where the Lorentz Force is negligible, the gas pressure must be hydrostatic with a single radial temperature profile. Since the gravitational term is small, the classical equilibrium solutions without gravity, as described in Appendices A and B, are applicable in every small volume, and equations (1 – 2) relevant as written, but with the allowance that quantities might vary slowly spatially. Thus we obtain coupled atmospheric and magnetic height variations as described in the introduction when isolated weak evacuated non-force-free flux tubes are present.

More generally with any hydrostatically connected non-force-free fields, the atmospheric and magnetic height variations must be coupled. Conditions along field lines are represented by a parallel-field equation, which is the projected component of the MHS equation (4) along \mathbf{B} ,

$$\mathbf{B} \cdot \left(\nabla p + \frac{p}{h} \nabla r \right) = 0. \quad (5)$$

The relation says that gas pressure changes along field lines must be hydrostatic, which can be seen by introducing an integrating factor ϕ into the gas pressure

$$p = \phi \hat{p}, \quad (6)$$

for an unrestricted function \hat{p} . Upon substitution

$$\mathbf{B} \cdot \left(\phi \nabla \hat{p} + \hat{p} \left(\nabla \phi + \frac{\phi}{h} \nabla r \right) \right) = 0, \quad (7)$$

so taking for the integrating factor

$$\nabla \ln(\phi) = -\frac{1}{h} \nabla r, \quad (8)$$

we obtain $\mathbf{B} \cdot \nabla \hat{p} = 0$, or \hat{p} constant along field lines. The only solutions to equation (8) are the 1D $\phi = \phi(r)$ and $h = h(r)$ or $T = T(r)$, represented in the hydrostatic relation

$$\frac{\partial \ln(\phi(r))}{\partial r} = -\frac{1}{h(r)}, \quad (9)$$

which can be integrated to give

$$\phi(r) = \exp \left(- \int_{r_\odot}^r \frac{dr}{h(r)} \right), \quad (10)$$

where r_\odot denotes an arbitrary base height for the radial variations. Thus pressure variations along arbitrarily directed field lines follow the 1D hydrostatic scale-height function $\phi(r)$ from a constant base pressure \hat{p} . 3D effects are possible because the base pressure \hat{p} and the scale-height function $\phi(r)$ or temperature profile $T(r)$ can vary from field line to field line. One scale-height function $\phi(r)$ with temperature profile $T(r)$ applies throughout force-free regions and in all hydrostatically connected non-force-free fields as we discuss at the end of this section.

Substituting equation (6) into the MHS equation (4) and using equation (8) gives the cross-field equation

$$\phi(r) \nabla \hat{p} = \frac{1}{4\pi} (\nabla \times \mathbf{B}) \times \mathbf{B}, \quad (11)$$

for \hat{p} allowed to vary from field line to field line. We adopt the single common scale-height function $\phi(r)$ assuming hydrostatic conditions are everywhere connected. At a base height r_\odot , $\phi(r_\odot) = 1$, and the cross-field equation (11) resembles the classical MHS equation (A.1) without gravity. Since the base height r_\odot is arbitrary, it is again evident that the classical equilibrium solutions must be applicable in every small volume.

Since the base pressure \hat{p} must be constant along field lines, the variations contained in the scale-height function $\phi(r)$ on the left side of equation (11) must be reproduced in the Lorentz Force or in \mathbf{B}^2 on the right side. Except for terms that arise due to the derivatives of the scale-height function, which are of order d/h , the variation of \mathbf{B} in non-force-free fields must go like $\phi(r)^{1/2}$ along field lines. Formally we can absorb $\phi(r)$ back into the magnetic field on the right side by decomposing \mathbf{B} into the general product

$$\mathbf{B} = \phi_B(r) \hat{\mathbf{B}} = \phi_{B2}(r)^{1/2} \hat{\mathbf{B}} = \phi(r)^{1/2} \zeta(r) \hat{\mathbf{B}}. \quad (12)$$

A 1D magnetic scale-height function $\phi_B(r)$ is sufficient to cancel $\phi(r)$; we introduce the residual radial multiplier $\zeta(r)$ to allow differing scale-height functions leaving $\hat{\mathbf{B}}$ an unrestricted vector function. Substituting back into equations (3 – 4) eliminates $\phi(r)$

$$\nabla \cdot (\zeta(r) \hat{\mathbf{B}}) = \frac{1}{2h(r)} \nabla r \cdot \zeta(r) \hat{\mathbf{B}}, \quad (13)$$

$$\nabla \hat{p} = \frac{1}{4\pi} \left(\left(\nabla - \frac{\nabla r}{2h(r)} \right) \times (\zeta(r) \hat{\mathbf{B}}) \right) \times \zeta(r) \hat{\mathbf{B}}. \quad (14)$$

The equations can be solved by substituting perturbative expansions in powers of the small quantity $d/h(r)$, $\hat{p} = \sum_n \hat{p}_n (d/h(r))^n$ and $\hat{\mathbf{B}} = \sum_n \hat{\mathbf{B}}_n (d/h(r))^n$ for $n \geq 0$ with d a constant characteristic flux-tube thickness. The expansions separate according to powers of $(d/h(r))^n$ giving the zero-order equations

$$\nabla \cdot (\zeta(r) \hat{\mathbf{B}}_0) = 0, \quad (15)$$

$$\nabla \hat{p}_0 = \frac{1}{4\pi} (\nabla \times (\zeta(r) \hat{\mathbf{B}}_0)) \times (\zeta(r) \hat{\mathbf{B}}_0). \quad (16)$$

Equations (15 – 16) in \hat{p}_0 and $\zeta(r) \hat{\mathbf{B}}_0$ are equivalent to the classical MHS equations (3 and A.1) without gravity discussed in Appendix A. Thus the lowest-order solutions are just the classical equilibria, which exhibit a degenerate direction z in the local coordinate system (x, y, z) taken to be arbitrarily oriented with respect to the radial r . If the magnetic field has a radial projection with $z \not\perp r$, any variations in z introduced by $\zeta(r)$ must be compensated in $\hat{\mathbf{B}}_0$. There is no loss in generality in taking $\zeta(r) = 1$ and $\phi_{B2}(r) = \phi(r)$ leaving $\hat{\mathbf{B}}_0$ equivalent to the unperturbed solution from equation (A.6) and constant in z .

Strictly the limiting case considered by Dungey (1953) where all field lines are perpendicular to the radial direction is not covered by our argument. With $z \perp r$, the component $\zeta(r) \hat{\mathbf{B}}_0$ can be independent of z without $\zeta(r)$ being constant. Magnetic distortion effects are introduced and specific minimally distorted solutions might be obtained as described in the introduction. Since the purely perpendicular case is singular, the result that $\phi_{B2}(r) = \phi(r)$ in equation (12) must still be satisfied in general. Thus $h_B(r) = 2h(r)$ at every r , where the magnetic scale height is defined in the usual way $h_B(r) = -[\partial \ln(\phi_B(r)) / \partial r]^{-1}$. The scale heights are coupled in all hydrostatically connected non-force-free MHS equilibria in a perturbing gravitational field.

The added perturbative terms developed in Appendix C give base functions \hat{p} and $\hat{\mathbf{B}}$ that weakly depend upon r . Radial variations enter $\hat{\mathbf{B}}$ due to the two small terms $\nabla r / (2h(r))$ in equations (13 – 14). The term on the right side of equation (13) is needed since a slow radial decrease in $|\mathbf{B}|$ cannot occur without a divergence of field lines; the term represents a compensating creation of flux in $\hat{\mathbf{B}}(r)$ with r . The small term added to the curl in the Lorentz Force in equation (14) originates with the rescaling of the magnetic field vector in r also. It corresponds to a small residual pseudo-force directed between $\hat{\mathbf{B}}$ and the outward radial ∇r . Such a term arises with a progressive left-handed rotation in the field lines at the rate of 1 radian in every magnetic scale height $2h(r)$. In MHS equilibria in a perturbing gravitational field, the amplitude, the divergence, and the curl of \mathbf{B} all vary on the large scale $2h(r)$.

One hydrostatic atmosphere must exist in every local plane of the magnetic field and current density, since equation (4) projected along lines of the current density, $\mathbf{J} = (c/(4\pi)) \nabla \times \mathbf{B}$, gives a relation like equation (5) with a different base pressure. Overlapping local planes between adjacent regions give connected hydrostatic equilibria, which must share a common temperature profile. It is postulated that hydrostatic regions of differing temperature can stably exist side-by-side if shielded by special arrangements of non-force-free fields and currents

(Kaiser & Salat, 1994; Boozer, 1998). Dark and bright threads are probably isolated thin flux tubes aligned with the background magnetic field embedded in current sheets suggestive of a bimodal amplitude distribution as discussed in Appendix B. Many conditions may connect flux-tube equilibria to the force-free region: a superposed planar current, a field component directed away from the flux tube due to its expansion with height, or fields changing in direction a small amount within an allowed field flexibility. Indeed the temperature in bright threads was found to be the same as the external ambient within observational uncertainties (November & Koutchmy, 1996).

In principle a single hydrostatically connected flux tube somewhere in the atmosphere fixes the scale height for the entire surrounding atmosphere, but all hydrostatically connected non-force-free magnetic fields must be consistent to satisfy mutually the horizontal pressure boundary condition. Differing radial variations in the background magnetic field at locations of flux tubes might be compensated with steady flux-tube flows.

Full 3D temperature effects seem possible in complex magnetic topologies, as in sunspots or prominences. In magnetically shielded regions, the internal gas pressure need not follow the external $p_i(r) \neq p_e(r)$. If the shielded flux tube is cooler than the surrounding ambient, $p_i(r)$ exhibits a more rapid exponential decline than $p_e(r)$, and the flux tube tends to become evacuated with height with $p_e(r) - p_i(r)$ tending to $p_e(r)$. With a reduced field strength $|\mathbf{B}_i(r)| < |\mathbf{B}_e(r)|$, the variation becomes incommensurate with the equilibrium conditions at some height. For hot flux tubes, $p_i(r) - p_e(r)$ tends to $p_i(r)$ with height. With reduced field strength the variation $p_i(r) \propto \mathbf{B}_e(r)^2$ represents just the same temperature as the normal surroundings, and with excess field strength the internal pressure of the hot flux tube $p_i(r)$ becomes incommensurate with the equilibrium conditions at some height. Of course inconsistent conditions may be avoided if the flux-tube temperature relation varies with height or exists in height-limited closed field configurations.

Continuous 3D non-force-free equilibrium solutions are claimed (Low, 1985, 1991), but these allow an arbitrary hydrostatic 1D gas pressure independent of the magnetic field (see the use of $p_0(r)$ and discussion around equation (24) of Low 1991, in §III in Bogdan & Low 1986, or §4 in Neukirch 1997). In the general force balance in the cross-field equation (11) with $\phi(r)$ allowed to vary from field line to field line, the pressure and magnetic variations cannot be separated except in force-free regions unconstrained by a horizontal pressure boundary condition, or containing only hydrostatically disconnected non-force-free fields.

We have confined our study here to the static solutions, but it is straightforward to broaden consideration to include certain types of steady flows. Steady flows give two types of contributions to the steady acceleration term, which appears in the more general steady equilibrium equation, corresponding to a flow pressure and a cross force, using the vector identity $\rho \mathbf{u} \cdot \nabla \mathbf{u} = \rho \nabla \mathbf{u}^2 / 2 + \rho (\nabla \times \mathbf{u}) \times \mathbf{u}$. The flow pressure adds a new term to the parallel-field equation (5), which leads to a hydro-steady relation in place of equations (9 – 10), but the same cross-field equation (11) results. The cross force gives a contribution to the Lorentz Force for isolated flows along flux

tubes. Since neither of these effects modify the basic form of the equilibrium relation equation (11), we obtain equilibrium solutions exhibiting a gas pressure containing atmospheric and wind components coupled to the average external magnetic field near flux tubes, which might possibly be modified by flux-tube flows.

Uniform radial wind flows in a force-free or parallel-field hydro-steady relation exhibit a quite different run of temperature for a given radial run of gas pressure than those derived based upon the hydrostatic relation equation (9). For a given scale-height function $\phi(r)$, as might be defined by the magnetic field in a magnetically dominated regime like a lower stellar corona, the atmospheric part of the scale height $h(r)$ and corresponding temperature $kT(r) = \bar{m}g(r)h(r)$ are always larger with a steady flow than without (Parker, 1960).

3. Model Atmospheres

The derivation of an explicit static equilibrium solution is a formidable task, because such an analysis must consider the specific form that distorted magnetic fields take in the presence of a gas. However an approximate flux-remapping common scale-height function can be written

$$\tilde{\phi}(r) = \phi_a(r) + \frac{1}{\beta_\odot} \phi_{B2}(r), \quad (17)$$

where $\phi_a(r)$ and $\phi_{B2}(r)$ are nominal separate gas and magnetic pressure solutions normalized at a base height r_\odot . The atmospheric-pressure scale-height function $\phi_a(r)$ represents a nominal hydrostatic solution for the gas alone, i.e. equation (9) with a temperature found by using a transfer equation that represents all of the usual energetic inputs and losses. The magnetic scale-height function $\phi_{B2}(r)$ represents the magnetic energy density near a representative flux tube for a nominal unperturbed magnetic field, i.e. a spherical potential field. The gas to magnetic pressure contribution at r_\odot is defined by β_\odot ; $1/\beta_\odot^{1/2}$ can be interpreted as the relative area covered by magnetic fields in evacuated flux tubes at the base surface. We restrict consideration to just static solutions here.

At a base height r_\odot , which we take as the stellar photospheric surface, only a small fraction of the area is occupied by magnetic fields in isolated flux tubes, $\beta_\odot \gg 1$ and $\tilde{\phi}(r) \simeq \phi_a(r)$. The gas pressure is dominant and must follow its nominal atmospheric form not being much affected by the magnetic field, whereas the magnetic field lines must be highly distorted. The atmospheric contribution $\phi_a(r)$ characteristically falls off much more rapidly than the magnetic pressure $\phi_{B2}(r)$, so around some transition height r_t where $\phi_a(r_t) = \phi_{B2}(r_t)/\beta_\odot$, $\tilde{\phi}(r)$ changes from $\phi_a(r)$ to $\phi_{B2}(r)/\beta_\odot$ over about one gas-pressure scale height. Above r_t the magnetic field is dominant, $\tilde{\phi}(r) \simeq \phi_{B2}(r)/\beta_\odot$, and the field must follow its nominal form irrespective of the gas pressure. There the gas pressure profile is very distorted from the nominal representing an added atmospheric heating caused by quasi-steady dynamics as we discuss §4.

Both the magnetic and gas pressure variations must be distorted from their nominal separate forms in the intermediate transition region. As an approximation, we assume that

the total pressure $p + \mathbf{B}^2/(8\pi)$ is preserved in the thin transition region, which gives an approximate flux-conserving extrapolation below the magnetically dominated corona and a gas-pressure-preserving extrapolation above the photosphere. The total relative pressure in the transition region goes from $A_T(\phi_a(r) + \phi_{B2}(r)/\beta_\odot)$ for a nominal superposition of independent gas and magnetic pressures $\phi_a(r)$ and $\phi_{B2}(r)/\beta_\odot$ with A_T the total surface area, to $(A_T - A_e)\tilde{\phi}(r) + A_B\tilde{\phi}(r)$ for the common pressure $\tilde{\phi}(r)$ with A_e the evacuated area and A_B the magnetically filled area. The two pressure totals are equal in general only with $\tilde{\phi}(r)$ from equation (17) and when the field-filling regions are evacuated with $A_B = A_e$. Anyway the choice of common scale-height function is not critical as smooth switching functions with correct asymptotic behavior in the photosphere and corona exhibit very similar temperature profiles even in the transition region.

For demonstration purposes, we take $\phi_a(r)$ to follow a polytrope power law

$$\phi_a(r) = \left(\frac{r_\odot}{r}\right)^{\eta+1}, \quad (18)$$

where η is the polytrope index. The hydrostatic relation equation (9) gives $h = r/(\eta+1)$, and from the definition $h = p/(\rho g)$, $\rho \propto \phi_a(r)r \propto \phi_a(r)^{\eta/(\eta+1)} \propto p^{\eta/(\eta+1)}$, which is the familiar thermodynamic relation for polytropes. A representative atmospheric surface temperature T_\odot defines the surface scale height h_\odot , and the polytrope index $\eta = \bar{m}g_\odot r_\odot/(kT_\odot) - 1$.

Similarly $\phi_{B2}(r)$ can be taken for single-harmonic potential magnetic field. The potential magnetic form seems to be consistent with what is observed in the lower solar corona for $r < 1.6r_\odot$ (Altschuler & Newkirk, 1969; Schatten et al., 1969). The potential magnetic field vector is the gradient of a sum of scalar spherical-harmonic component functions, each of which is the separable product of a 2D surface function and radial multiplier $1/r^{\ell+1}$. The resulting magnetic field in each spherical harmonic component goes like $1/r^{\ell+2}$ in all its vector elements; a monopole $\ell = 0$ exhibits a r^{-2} radial falloff, a dipole field $\ell = 1$, a r^{-3} falloff, etc. For a single spherical harmonic ℓ the magnetic energy density falls off like

$$\phi_{B2}(r) = \left(\frac{r_\odot}{r}\right)^{2\ell+4}. \quad (19)$$

With a superposition of spherical harmonics, a nonuniform radial dependence can occur, and a representative average spherical harmonic ℓ might be obtained by appropriately weighting flux-tube locations.

The temperature is written from the hydrostatic relation equation (9)

$$kT(r) = \bar{m}g(r)h(r) = -\bar{m}g(r) \left(\frac{1}{\phi(r)} \frac{\partial \phi(r)}{\partial r} \right)^{-1}. \quad (20)$$

Taking $\phi(r)$ to be $\tilde{\phi}(r)$ from equation (17) with $\phi_a(r)$ from equation (18) and $\phi_{B2}(r)$ from equation (19), we obtain an explicit formula for $T(r)$. In the corona $\phi(r) \simeq \phi_{B2}(r)/\beta_\odot$, the formula exhibits the limiting scale height

$$h_{\text{cor}}(r) = \frac{r}{2\ell+4}, \quad (21)$$

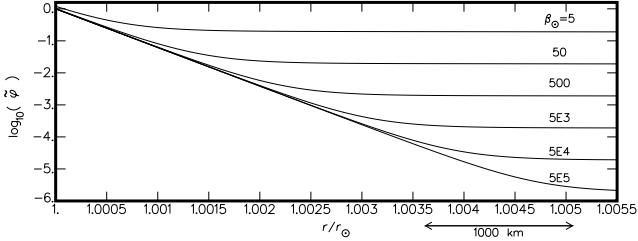


Fig. 2. Log of scale-height function $\log_{10}(\tilde{\phi}(r))$ for solar polytrope of reference temperature $T_\infty = 3800$ °K and a potential magnetic field $\ell = 2.4$ with different β_∞ .

and temperature

$$kT_{\text{cor}}(r) = \frac{GM_\odot \bar{m}}{(2\ell + 4)r}. \quad (22)$$

The limiting base coronal temperature $T_{\text{cor}}(r_\odot)$ is defined entirely by the stellar surface gravity, radius, and main magnetic spherical harmonic. For a toroidal field $\ell = 2$ the scale height at the stellar surface is $h_{\text{cor}}(r_\odot) = r_\odot/8$, giving a solar base coronal temperature of $T_{\text{cor}}(r_\odot) = 1.73 \times 10^6$ °K using $\bar{m} = 0.6m_p$ for m_p the proton mass ($\bar{m} = 1 \times 10^{-24}$ g, $r_\odot = 6.96 \times 10^{10}$ cm, $g_\odot = 2.75 \times 10^4$ cm s⁻², and $k = 1.38 \times 10^{-16}$ ergs/°K). With the solar base coronal temperature of $T_{\text{cor}}(r_\odot) = 1.6 \times 10^6$ °K, we obtain the spherical harmonic $\ell = 2.4$.

Figure 2 shows some examples of the scale-height function $\tilde{\phi}(r)$ from equations (17 – 19) in the lowest part of the solar atmosphere around the transition height r_t . Scale-height functions are plotted for a range of β_∞ with a polytrope of reference surface temperature $T_\infty = 3800$ °K, and spherical harmonic $\ell = 2.4$, for the solar radius, surface gravity, and mean particle mass. As all of the curves are based on the same polytrope, they coincide until the transition height r_t for the model is reached and then switch rapidly to the nominal magnetic $\phi_{B2}(r)$, which appears to be relatively flat on the log scale.

The radial expansion of a flux tube is another way to visualize the field strength decrease in the atmosphere and the properties of the common scale-height function. Figure 3 portrays flux-tube diameter as a function of height r for solar polytropes with reference temperatures T_∞ and field strengths β_∞ . For conservation of the total flux through the cross-sectional area of a flux tube $\pi(d/2)^2|\mathbf{B}|$, the flux-tube diameter $d(r)$ must increase with radial distance r , $d(r) \propto |\mathbf{B}|^{-1/2} \propto \phi(r)^{-1/4}$.

For a given polytrope, all flux tubes exhibit approximately the same shape up to a height that depends upon β_∞ , a lower canopy top and less overall relative expansion being found with a higher magnetic surface coverage as for sunspots. The turning height is somewhat below the location of the fastest temperature change due to the differing dependencies: The field strength, which goes like $\phi(r)^{1/2}$, turns from the atmospherically determined form at r_t , but the most rapid temperature change occurs significantly higher where the slope of the scale-height function flattens out as $T(r) \propto -[\partial \ln(\phi(r))/\partial r]^{-1}$.

Figure 4 shows the temperature variation in a lower solar atmosphere using equation (20) for the scale-height function from equations (17 – 19). The upper panel shows the model atmospheres for $\ell = 2.4$ and $\beta_\infty = 5000$ with different polytropes,

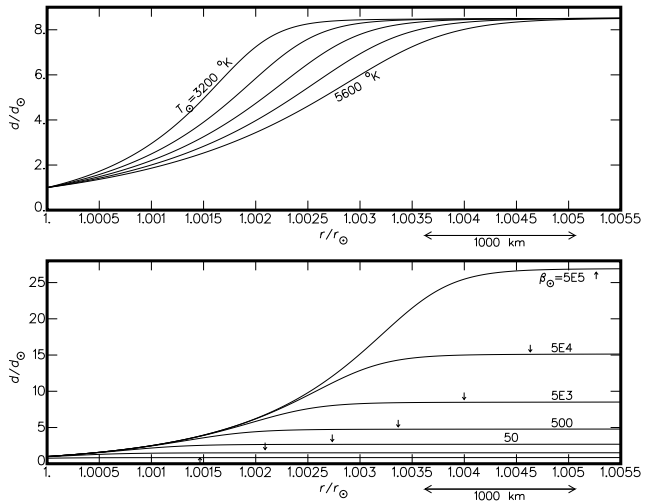


Fig. 3. Relative flux-tube diameter $d(r)/d(r_\odot)$ in lower solar atmosphere for $\ell = 2.4$ and $\beta_\infty = 5000$ for solar polytropes of reference temperatures $T_\infty = 3200$ °K, 3800 °K, 4400 °K, 5000 °K, and 5600 °K, (upper panel) and for $\ell = 2.4$ and $T_\infty = 3800$ °K with $\beta_\infty = 0.5, 5, 50, 500, 5E3, 5E4$, and $5E5$ (lower panel). The arrow on each curve locates the most rapid temperature change for the model.

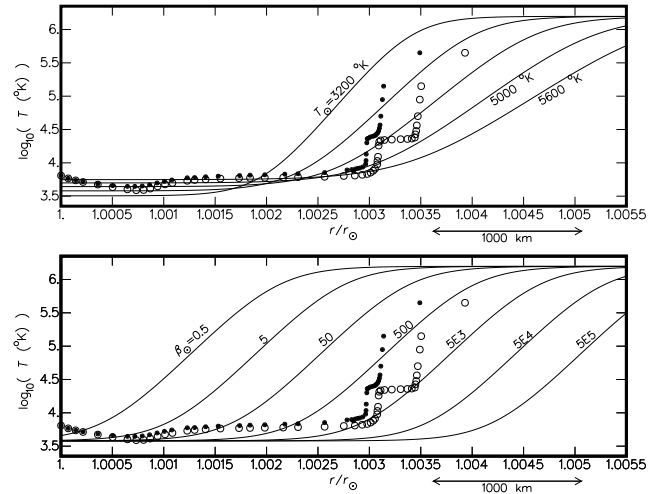


Fig. 4. Log of lower solar atmosphere $\log_{10}(T(r))$ for $\ell = 2.4$ and $\beta_\infty = 5000$ for polytropes with $T_\infty = 3200$ °K, 3800 °K, 4400 °K, 5000 °K, and 5600 °K (upper panel), and for $\ell = 2.4$ and $T_\infty = 3800$ °K with different β_∞ (lower panel), both shown with the solar VAL A (open circles) and F (filled circles) model temperatures.

and the lower panel the model atmospheres for $\ell = 2.4$ and $T_\infty = 3800$ °K with different β_∞ . Temperatures from the VAL A and F models are shown corresponding to cool inner network and hot network bright points, respectively (Vernazza et al., 1981).

In the solar photosphere, the nominal atmospheric polytrope exhibits an approximately constant temperature. Of course the features of the real solar atmosphere can never be well approximated by a polytrope. The shape of the temper-

ature function through the chromosphere and transition region, where the scale-height function $\tilde{\phi}(r)$ goes from $\phi_a(r)$ to $\phi_{B2}(r)/\beta_\odot$, depends upon the polytrope index and surface field strength β_\odot but not on the spherical harmonic ℓ , which separately determines the base coronal temperature. Solar models using polytropes with reference surface temperatures near the photospheric minimum $T_\odot = 3800$ °K and $\beta_\odot \approx 5000$ or ≈ 500 most accurately reproduce the transition-region heights and thicknesses for the VAL A or F models, respectively. The more recent solar atmospheric model of Fontenla et al. (1990) corrects to remove particle diffusion effects and exhibits a much more abrupt transition region than what is predicted here. However the tendency for equilibrium to be restored in a near equilibrium atmosphere may preclude diffusion effects and other dissipative processes as discussed in §4.

For the maximum flux-tube evacuation in the solar photosphere $\mathbf{B}(r_\odot)^2 = 8\pi p(r_\odot)$, we obtain a field strength of $|\mathbf{B}(r_\odot)| = 1715$ Gauss using $p(r_\odot) = 1.17 \times 10^5$ dynes cm⁻² from the VAL models. The relative flux-tube areal coverage is defined as $1/\beta_\odot^{1/2}$, 1/71 for $\beta_\odot = 5000$ and 1/22 for $\beta_\odot = 500$. When flux tubes fully expand to fill the coronal surface area, the average field strength goes like $\mathbf{B}_{\text{cor}}^2 = 8\pi p(r_\odot)/\beta_\odot$ giving $|\mathbf{B}_{\text{cor}}| = 24$ Gauss for $\beta_\odot = 5000$ and $|\mathbf{B}_{\text{cor}}| = 76$ Gauss for $\beta_\odot = 500$, not out of range for solar coronal observations (Lin et al., 2000). The models exhibit the known tendency for a lower transition region to occur near active regions where the photospheric flux-tube area coverage and coronal magnetic field strength are larger.

Figure 5 illustrates the solar atmospheric temperature function $T(r)$ for various ℓ with the coronal temperatures inferred from the white-light-intensity radial gradient taken from eclipse photographs (Newkirk et al., 1970) and inferred from FeXIV 5303Å line-width measurements (Jarrett & von Klüber, 1958). The limited resolution in r in the figure hides the transition region near r_\odot . The coronal model for the spherical harmonic $\ell = 1$ seems to give the best overall agreement with the measured radial profiles, but $\ell = 2.4$ better matches the base coronal temperature. However all of the model curves show a more rapid falloff than the measured temperature profiles. Models containing an outward wind should give systematically higher temperatures with height in the corona. The average spherical harmonic in active regions should be larger due to the complexity of magnetic fields in those regions suggesting that base coronal temperatures might actually be lower there; a cooler lower-temperature active-region component is a possibility in solar coronal observations (Guhathakurta et al., 1994).

4. Near Equilibrium Processes

Equilibria are naturally self restoring. In the absence of sufficient external gas or flow pressure, a time-dependent outward gas acceleration outside rigidly held non-force-free flux tubes arises in the overall MHD balance, which acts generally to reestablish equilibrium.

Coronal energy losses due to dissipative processes or steady outflows tend to cool the atmosphere and reduce the common pressure scale height, geometrically stressing the magnetic state, which contributes to magnetic instability. When

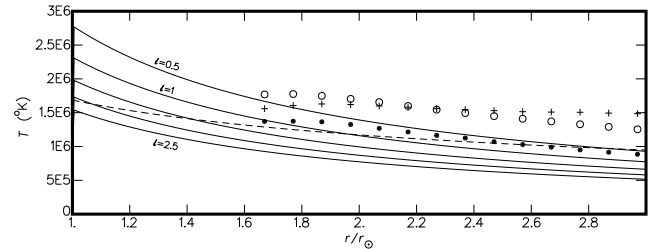


Fig. 5. Static solar corona $T(r)$ for $\ell = .5, 1, 1.5, 2$, and 2.5 (from top to bottom) shown with temperature from white-light intensity in the quiet equator (filled circles), in SW (crosses), and in SE (open circles) streamers (Newkirk et al., 1970), and from line-width measurements (dashed line) (Jarrett & von Klüber, 1958).

magnetic collapses are fast compared to evolutionary processes and the magnetic field dominant over the gas, the quasi-steady approximation is applicable and MHD equilibria are catastrophically self restoring (Low, 1977). Catastrophic magnetodynamics in a perturbed configuration produce collapses to new stable magnetic states on Alfvén-velocity transit times in solar flare scenarios. With a renewed magnetic state, outflows reestablish the equilibrium gas-pressure profile of the depleted cool atmosphere heating the gas compressively, as we describe in Appendix D for the limiting case when magnetodynamics are fast compared to the hydrodynamics. Thus MHD processes in the quasi-steady limit naturally produce outflows along field lines, a ‘magnetic suction’. The basic phenomenon may be important in other problems in physics and astrophysics, but discussion lies beyond the scope of this paper.

Restoring flows along field lines seem in evidence in the vicinity of coronal voids (Wagner et al., 1983), may take the form of spicule eruptions in the solar photosphere or supergranular-scale chromospheric outflows as inferred from post-flare spectral-line blue shifts (Schmieder et al., 1987; Cauzzi et al., 1996). The upward total mass flux contributed by solar spicule events is about 100 times the total wind mass flux but represents only a small fraction of the total wind energy flux (Pneuman & Kopp, 1978).

The energy required to lift the gas to restore and heat a depleted atmosphere or drive an outward wind must come out of the total energy supplied to the magnetic field due to new flux coming up from the convection zone below or to local mechanical inputs from photospheric twisting and flux-tube motions. If sufficient magnetic energy is not available to offset losses, then force-free equilibria possibly containing sheathed non-force-free fields are the only possibility. Magnetic adjustments are made much more effective through the coupling of the gas to the magnetic field and may thereby indeed be the principle mechanism for coronal heating. Post-reconnection hydrodynamic heating acting everywhere throughout the coronal volume overcomes the often-cited difficulty that reconnection events are so spatial localized and short-lived that only a larger event rate than what can be directly inferred from observations could account for coronal heating (Heyvaerts & Priest, 1984; Hudson, 1991).

The remarkable feature of an MHS corona containing isolated weak evacuated flux tubes or hydrostatically connected non-force-free fields is that the temperature is essentially a geometric parameter defined by the stellar surface gravity, radius, and main magnetic spherical harmonic from equation (22) with $r = r_\odot$. The observed solar base coronal temperature of 1.6×10^6 K is predicted with a spherical harmonic $\ell = 2.4$ consistent with the large-scale solar magnetic field, which exhibits substantial power in the toroidal $\ell = 2$ and spherical harmonics $\ell = 3$ or 4 as evidenced by the presence of active longitudes. Our formula for the base coronal temperature equation (22) has been suggested already in the hypothesis of a ‘geometric boundary condition’ relevant when the individual particle energy or temperature is related to the surface potential (Menzel, 1968; Scudder, 1992); the formula gives accurate coronal temperatures for a range of stellar types (Williams & Mullan, 1996).

Acknowledgements. The author is grateful to many for useful discussion during the course of this work, and especially to Eric Priest and Ray Smartt for their careful reviews of the manuscript.

Appendix A: Local MHS Equilibria

There are well-known solutions to the classical static problem describing a gas existing in conjunction with elongated magnetic fields without a perturbing gravitational field (Parker, 1979, Chapter 6). It is helpful to revisit the classical problem here in a general way. The classical MHS equilibrium equations without gravity are Gauss’ Law, equation (3), and the static equilibrium equation

$$\nabla p = \frac{1}{4\pi}(\nabla \times \mathbf{B}) \times \mathbf{B}. \quad (\text{A.1})$$

Plane-parallel solutions can be developed based upon the general Cartesian vector function

$$\mathbf{B} = \left(\frac{\partial a(\mathbf{x})}{\partial y}, -\frac{\partial a(\mathbf{x})}{\partial x} - \frac{\partial b(\mathbf{x})}{\partial z}, \frac{\partial b(\mathbf{x})}{\partial y} \right), \quad (\text{A.2})$$

The x and z vector components of \mathbf{B} , $\partial a/\partial y$ and $\partial b/\partial y$, are taken to be unrestricted functions, and the y component is written so that equation (3) is always satisfied. It is convenient to use derivative forms in the vector components to avoid complicating integrals.

Any solutions to equation (A.1) must satisfy the two conditions $\mathbf{B} \cdot \nabla p = 0$ and $(\nabla \times \mathbf{B}) \cdot \nabla p = 0$, which are rewritten using \mathbf{B} from equation (A.2)

$$C_{xy}a - C_{yz}b = 0, \quad (\text{A.3})$$

$$\left(C_{xz} \frac{\partial}{\partial x} + C_{yz} \frac{\partial}{\partial y} \right) a + \left(C_{xy} \frac{\partial}{\partial y} + C_{xz} \frac{\partial}{\partial z} \right) b = 0, \quad (\text{A.4})$$

using the linear commutation operators $C_{xy} = (\partial p/\partial x)(\partial/\partial y) - (\partial p/\partial y)(\partial/\partial x)$, etc., which contain $p(\mathbf{x})$ as an implicit function.

The two equations (A.3 – A.4) can be used to write two of the functions in terms of the third, e.g. $a(\mathbf{x})$ and $b(\mathbf{x})$ in terms of $p(\mathbf{x})$. Fourier integrating the coupled equations and combining

gives one 2×2 matrix integral equation over the 3D wavenumber domain \mathbf{j}

$$\int \begin{pmatrix} c_{xy} & -c_{yz} \\ c_{xz}j_x + c_{yz}j_y & c_{xy}j_y + c_{xz}j_z \end{pmatrix} \begin{pmatrix} \bar{a}(\mathbf{j}) \\ \bar{b}(\mathbf{j}) \end{pmatrix} d^3j = 0, \quad (\text{A.5})$$

where the commutation operators have become the simple commutator factors $c_{xy} = \bar{p}(\mathbf{k} - \mathbf{j})((k_y - j_y)j_x - (k_x - j_x)j_y)$, etc., and the integral is a function of wavenumber \mathbf{k} ; the Fourier functions $\bar{a}(\mathbf{k})$, $\bar{b}(\mathbf{k})$, and $\bar{p}(\mathbf{k})$ are defined as usual, $\bar{a}(\mathbf{k}) = \int a(\mathbf{x}) \exp(i\mathbf{k} \cdot \mathbf{x}) d^3x$, etc. The integral represents a form of inner product in \mathbf{j} between $\bar{p}(\mathbf{k} - \mathbf{j})$ times a matrix containing quadratic polynomials in \mathbf{j} , which depend upon \mathbf{k} , and a vector that is a function of \mathbf{j} alone. For the integral to vanish, the matrix and vector functions must be orthogonal. As orthogonality is required for all shifts \mathbf{k} , the only non-trivial possibility is that one of the inner-product terms be zero, meaning that a necessary condition for nontrivial solutions is that the matrix determinant in equation (A.5) vanish, or with rearrangement $c_{xy}^2 + c_{yz}^2 + c_{xz}^2 = 0$. The determinant relation applies at every (\mathbf{j}, \mathbf{k}) , so combining conjugate relations and using the Hermitian property $\bar{p}(\mathbf{k})^* = \bar{p}(-\mathbf{k})$, we obtain $|c_{xy}|^2 + |c_{yz}|^2 + |c_{xz}|^2 = 0$. Thus $c_{xy} = c_{yz} = c_{xz} = 0$, corresponding to $C_{xy} = C_{yz} = C_{xz} = 0$ in equations (A.3 – A.4).

Taking all the commutator operators to vanish but without other reduction, $a(\mathbf{x})$, $b(\mathbf{x})$, and spatial derivatives of $a(\mathbf{x})$ and $b(\mathbf{x})$ must be functions of $p(\mathbf{x})$ alone in equations (A.3 – A.4), which is only possible for certain trivial spatial forms for real functions, so other reductions are required. Taking $\partial/\partial z = 0$ gives a consistent solution defined by the functional dependences $a = a(p(x, y))$ in equation (A.3) and $\partial b/\partial y = (\partial b/\partial y)(p(x, y))$ in equation (A.4). A similar solution is obtained by taking $\partial/\partial x = 0$. These two solutions or linear combinations are equivalent with rotation of the $x - z$ axes around y . Taking z as the degenerate direction reduces the possibilities to one general solution, ordinarily written with a as the implicit function

$$\mathbf{B} = \left(\frac{\partial a(x, y)}{\partial y}, -\frac{\partial a(x, y)}{\partial x}, B_z(a(x, y)) \right). \quad (\text{A.6})$$

The degenerate z is a direction of field elongation. The magnetic potential function $a(x, y)$ defines a 2D planform for the solutions, which determines the spatial variations in the longitudinal field component $B_z = B_z(a(x, y))$ and gas pressure $p = p(a(x, y))$ as arbitrary 1D mappings. The magnetic field is everywhere perpendicular to the gradient of $a(x, y)$, since $\mathbf{B} \cdot \nabla a(x, y) = 0$.

It is widely believed anyway that the 2D solution is the only plane-parallel one. Using perturbative expansions, Parker shows that no nearby 3D solutions exist for bounded quantities in an infinite domain (Parker, 1979, Section 14.2). However 3D variations do arise as large-scale deviations from plane parallel (Arendt & Schindler, 1988). In the common shorthand, ‘2.5D’ solutions refer to perturbed solutions in the problem with gravity, which admits large-scale variations in the degenerate direction of the magnetic field.

Appendix B: Properties of Local MHS Equilibria

Substituting \mathbf{B} from equation (A.6) into equation (A.1) gives the governing equation for the implicit magnetic potential function $a(x, y)$ for the static equilibrium problem without gravity

$$\left(\nabla^2 a + \frac{d}{da} \left(4\pi p(a) + \frac{B_z(a)^2}{2} \right) \right) \nabla a = 0. \quad (\text{B.1})$$

Where $\nabla a \neq 0$, the potential function must satisfy the Grad-Shafranov (GS) Equation, written

$$\nabla^2 a(x, y) = -P'(a(x, y)), \quad (\text{B.2})$$

defining the total pressure $P(a) = 4\pi p(a) + B_z(a)^2/2$, where $P'(a) = dP(a)/da$.

The total pressure $P(a)$ and its component functions $p(a)$ and $B_z(a)$ are all one dimensional and nonlinear but must all be well-defined everywhere in the solution domain consistent with their forms at the boundaries. Strictly, disagreeing z boundary conditions are inconsistent with the z independence of the solutions; differences might produce small deviations in the solutions like twist or divergence or be a source of dynamical instability. It is popular to restrict consideration to entirely force-free solutions with $p'(a) = 0$; the restriction does not change the nature of the basic GS equation (B.2) for $a(x, y)$ but requires the specific current density $\mathbf{J} = (c/(4\pi))B_z'(a)\mathbf{B}$ for an arbitrary $B_z(a)$, as is evident by expanding \mathbf{J} using \mathbf{B} from equation (A.6) with $\mathbf{J} \propto \mathbf{B}$.

The magnetic potential function a is constant everywhere in the local plane of \mathbf{B} and \mathbf{J} . From equation (A.1), $\mathbf{J} \cdot \nabla p(a) = 0$. Then $\mathbf{J} \cdot \nabla p(a) = (\mathbf{J} \cdot \nabla a) p'(a) = 0$. Thus $\mathbf{J} \cdot \nabla a = 0$ at least when $p'(a) \neq 0$, and when $p'(a) = 0$, $\mathbf{J} \parallel \mathbf{B}$ so $\mathbf{J} \cdot \nabla a = 0$ anyway. We think of a as constant on ribbon-like current sheets with possible embedded flux-tube anomalies along \mathbf{B} , the solution surfaces being more curved along \mathbf{J} as it is defined by the derivatives of \mathbf{B} .

The GS equation (B.2) has the unusual feature that it contains the 1D filter function $P'(a)$. For the linear case, $P'(a) = k_0^2 a$ with k_0 a constant wavenumber. The Fourier transform of equation (B.2) then gives a transform function $\tilde{a}(k_x, k_y)$ that is zero everywhere in its 2D wavenumber domain $\mathbf{k} = (k_x, k_y)$ except on the thin annulus at $|\mathbf{k}| = k_0$ where arbitrary complex values Hermitian in $\pm \mathbf{k}$ are allowed. Taking the Fourier transform back gives a potential function $a(x, y)$ that is the convolution of a spatial distribution of delta-function source points with a common Bessel-function radial kernel times an azimuthal factor. Boundary conditions on $a(x, y)$ constrain the azimuthal factor leading to possible planar solutions defined by all power at one azimuth or axisymmetric solutions with power uniformly distributed in azimuth consistent with our visualization of current sheets with embedded cylindrical flux tubes. Physical arguments show that nonlinear kernels are similarly constrained by boundary conditions (Vainshtein & Parker, 1986).

Random spatial distributions of a common GS kernel are nonlinear GS solutions too. We take the potential function $a(x, y)$ to be the convolution of a distribution of sources $D(x, y)$ with a common 2D kernel function $A(x, y)$, $a(x, y) = D(x, y) * A(x, y)$. The distribution is written $D(x, y) = \sum_j c_j \delta(x-x_j, y-y_j)$ counting sources j of varying strength c_j , where $\delta(x, y)$ denotes

the 2D delta function. For a spatially incoherent or random distribution D of equal strength sources with all $c_j = 1$, D raised to a power is D alone; for equal amplitude sources with $c_j = \pm 1$, D raised to an odd power is D alone. For an analytic nonlinear driver function $P(a)$, the convolution with an incoherent distribution in D of suitably restricted amplitudes factors out $P'(a) = P'(D * A) = D * P'(A)$ and the GS equation (B.2) reduces to the same GS equation but for the common kernel function $A(x, y)$. The flux tubes studied in November & Koutchmy (1996) appear to lie in the two preferential groupings of dark and bright threads suggesting a bimodal amplitude distribution of a common flux-tube kernel.

It is easily seen from equation (3) that the divergence of the left side of equation (2) must vanish; $\nabla \cdot (\mathbf{B}_e \cdot \nabla) \mathbf{B}_i(\mathbf{x}) = \mathbf{B}_e \cdot \nabla (\nabla \cdot \mathbf{B}_i(\mathbf{x})) = 0$ where the magnetic field without gravity $\mathbf{B}(\mathbf{x})$ is written as the sum of a constant background component \mathbf{B}_e and a varying component $\mathbf{B}_v(\mathbf{x})$, as $\mathbf{B}(\mathbf{x}) = \mathbf{B}_e + \mathbf{B}_v(\mathbf{x})$, so $\mathbf{B}_i(\mathbf{x}) = \mathbf{B}_e + \mathbf{B}_v(\mathbf{x}) = \mathbf{B}(\mathbf{x})$. Thus expanding the Lorentz Force and taking the divergence of the MHS equation (A.1) gives

$$\nabla^2 \left(p + \frac{B^2}{8\pi} \right) \simeq \frac{1}{4\pi} \nabla \cdot (\mathbf{B}_e \cdot \nabla) \mathbf{B}_i(\mathbf{x}) = 0. \quad (\text{B.3})$$

The approximate equality reflects a missing term that is of order $\mathbf{B}_v(\mathbf{x})^2$ and vanishingly small when $|\mathbf{B}_v(\mathbf{x})| = |\mathbf{B}_i(\mathbf{x}) - \mathbf{B}_e| \ll |\mathbf{B}_e|$. As Parker (1972) points out, linear gradients in the total pressure are precluded by the boundedness of the quantities in an infinite domain, so the vector quantities acted on by the divergence on both sides of the approximate equality must separately approximately vanish. With the vector on the left side of the approximate equality set to zero, equation (1) is obtained, and with the vector on the right side zero equation (2). Parker (1972) shows that equation (2) is valid to all orders of the varying magnetic field in perturbative expansions. Additional discussion on his perturbative proof is contained in Appendix C.

The Parker theorem reflects the separability of the classical equilibria in equation (A.6) in the degenerate direction of the magnetic field z . A constant magnetic field can only enter into the z vector element $B_z(a)$ without producing other ramifications, whereas an added offset in the x or y elements of $\mathbf{B}(\mathbf{x})$ requires adding a uniformly inclined plane to $a(x, y)$. Such a plane is precluded by the boundedness of $a(x, y)$: Low-wavenumber components in the Fourier domain needed to represent the added plane are at odds with the Fourier ring solutions for the linear GS equation (B.2) and also contrary to the form of a superposition of spatially compact axisymmetric nonlinear kernels.

Appendix C: Perturbative Expansions

The higher-order equations in the perturbative series developed from equations (13 – 14) are written for $\zeta(r) = 1$; from equation (13)

$$\nabla \cdot \hat{\mathbf{B}}_n = -\frac{1}{2d} (\nabla r \cdot \hat{\mathbf{B}}_{n-1}) \left(1 + 2(n-1) \frac{\partial h(r)}{\partial r} \right), \quad (\text{C.1})$$

for $n > 0$, and from the MHS equation (14)

$$\nabla \hat{p}_n - \frac{1}{4\pi} \sum_{j=0}^n (\nabla \times \hat{\mathbf{B}}_j) \times \hat{\mathbf{B}}_{n-j} = \frac{1}{8\pi d} \sum_{j=0}^{n-1} (\nabla r \times \hat{\mathbf{B}}_j) \times \hat{\mathbf{B}}_{n-j-1} \left(1 + 2j \frac{\partial h(r)}{\partial r} \right), \quad (\text{C.2})$$

for $n > 0$. The equations are linear in the successive terms \hat{p}_n and $\hat{\mathbf{B}}_n$ based upon the lower-order terms. The zero-order base functions \hat{p}_0 and $\hat{\mathbf{B}}_0$ are 2D and constant in the degenerate magnetic field direction z ; higher-order terms may introduce 3D effects from the function $h(r)$ if r has a component along z . As required for consistency, $\hat{\mathbf{B}}_0 \cdot \nabla \hat{p}_0 = 0$ is the zero-order component of $\mathbf{B} \cdot \nabla \hat{p} = 0$.

A wide latitude is allowed for choosing perturbative quantities and as long as they are relatively small most everywhere the standard procedure remains valid. Van Ballegooijen (1985) questions the Parker (1972) choice of perturbative quantity and equation separation procedure, but Van Ballegooijen's assigning of approximate magnitudes to individual factors in his paper to separate his equations is not an algebraic procedure, and his resulting equations have inherent contradictions (Parker, 1987). Parker (1972) does not ascribe a particular functional meaning to his kernel ϵ as he says at the beginning of his §II: "Expand the field \mathbf{b} and pressure p in ascending powers of *some* parameter ϵ , which is of the order of $\epsilon = |\mathbf{b}|/|\mathbf{B}|$ " where \mathbf{b} is the small spatially varying magnetic field on the uniform background field \mathbf{B} . Our choice for perturbative kernel $d/h(r)$ with d constant leads to a convenient separation of orders.

The perturbative procedure is a functional separation method rooted in the natural independence of the basis functions ϵ^n irrespective of their real amplitudes. If the parameter ϵ is small almost everywhere the series solutions will be convergent. It may be true as Van Ballegooijen contends that there could be locations where the amplitude of some normally small expansion parameter ϵ actually becomes relatively large. These series expansions are divergent, but such behavior characteristically defines the isolated singularities of ordinary differential equations as discussed in theorems on the Frobenius method for series expansion.

Appendix D: Hydrodynamic Response to Fast Magnetic Adjustment

Equilibria tend to be self restoring even when magnetic fields are unstable, as we discuss in the case when the magnetic adjustment time is much shorter than the hydrodynamic adjustment time, which appears typical of many solar flares. Sporadic crossings of coronal loops in low-energy flare events (Lin et al., 1992) suggest 'X'-type configurations, and the instability of the 'X' configuration is well known to form a new current sheet at near the Alfvén velocity if a nonzero resistivity is affected in the region (Dungey, 1958; Syrovatskii, 1981); such a resistivity is predicted in some models (Petschek & Thorne, 1967; Priest, 1972). Taking a field strength of $B \simeq 400$ Gauss as representative of chromospheric magnetic fields near neutral lines in solar active regions where flares commonly occur, we obtain an Alfvén speed $c_a = B/(4\pi\rho)^{1/2} \simeq 10^8$ cm s $^{-1}$ (with $\rho = N\bar{m} = 10^{-12}$ g cm $^{-3}$ for $N = 10^{12}$ cm $^{-3}$ and $\bar{m} = 10^{-24}$ g). The Alfvén speed stays fairly constant into the corona giving a collapse time of $\tau_{\text{mag}} = h_B/c_a \simeq 160$ s for the propagation of the instability through a magnetic scale height $h_B = 2h_{\text{cor}} = r_{\odot}/4.4 \simeq 1.6 \times 10^{10}$ cm using a primary magnetic spherical harmonic of $\ell = 2.4$ in equation (21).

If the newly formed magnetic field contains non-force-free fields hydrostatically connected to the background force-free field, then the resulting Lorentz-Force term in the MHD equation must be balanced by pressure gradients and steady or time-dependent flows. The hydrodynamic problem can be represented in the projected component of the MHD equation along \mathbf{B} , which substitutes for a hydrostatic relation but leads to a constant cross-field balance like equation (11) as for the static or steady problems.

Dissipation effects enter the dynamical problem and may modify the timescales. However the energy equation is nearly adiabatic in solar coronal conditions since dissipative timescales are much longer than hydrodynamic timescales. The timescale for radiative dissipation is $\tau_{\text{rad}} = p/\Phi_{\text{rad}}$, where Φ_{rad} is the radiative loss rate. Taking for the solar corona $\Phi_{\text{rad}} \simeq (10^{-22}$ ergs cm 3 s $^{-1}$) $N_e N_H$ with N_e the electron density and N_H the hydrogen ion density (Cox & Tucker, 1969, figure 4), and using $N_e = N_H = N/2$, $N = 10^9$ cm $^{-3}$, and $T = 1.6 \times 10^6$ °K with $p = NkT$, gives $\tau_{\text{rad}} = 6400$ s. Timescales for the only other normal dissipative effects, viscous heating and heat diffusion, are about one or two orders of magnitude larger. Viscous effects are small as the relative order of the viscous term in the MHD equation is about 10^{-3} in solar coronal conditions.

An estimate for a nonturbulent hydrodynamic adjustment time can be obtained by linear analysis of the dynamical equation along field lines, perturbing the physical quantities backward in time from a final static or steady equilibrium state. In such analyses the time-dependent acceleration term balances the depleted pressure with an outflow from below that refills a depleted atmosphere to the equilibrium profile. In reestablishing the equilibrium pressure profile the gas is heated compressively and approximately adiabatically consistent with the energy equation. Characteristically the timescale for reaching equilibrium is the gravitational free-fall time through the scale height $\tau_{\text{hyd}} = (h/g(r_{\odot}))^{1/2}$, which is $\tau_{\text{hyd}} = 536$ s for the solar base-coronal scale height $h_{\text{cor}}(r_{\odot})$ defined by equation (21) with $\ell = 2.4$ and the solar radius.

References

- Altschuler, M. D. & Newkirk, G. J. 1969, Magnetic Fields and the Solar Corona: III. Methods of Calculating Coronal Fields, *Solar Phys.*, 9, 131–149
- Arendt, U. & Schindler, K. 1988, On the existence of three-dimensional magnetohydrostatic equilibria, *A&A*, 204, 229–234
- Bogdan, T. J. & Low, B. C. 1986, The three-dimensional structure of magnetostatic atmospheres. II - Modeling the large-scale corona, *ApJ*, 306, 271–283
- Boozer, A. H. 1998, What is a stellarator?, *Physics of Plasmas*, 5, 1647–1655
- Cauzzi, G., Falchi, A., Falciani, R., & Smaldone, L. A. 1996, Coordinated observations of solar activity phenomena. II. The velocity field pattern in an elementary flare., *A&A*, 306, 625–637
- Cheng, C. Z. & Choe, G. S. 1998, Current Sheets and Prominence Formation in the Solar Atmosphere, *ApJ*, 505, 376–389

Coles, W. A. & Harmon, J. K. 1978, Interplanetary scintillation measurements of the electron density power spectrum in the solar wind, *J. Geophys. Res.*, 83, 1413–1420

Cox, D. P. & Tucker, W. H. 1969, Ionization Equilibrium and Radiative Cooling of a Low-Density Plasma, *ApJ*, 157, 1157–1167

Dungey, J. W. 1953, A family of solutions of the magnetohydrostatic problem in a conducting atmosphere in a gravitational field, *MNRAS*, 113, 180–187

Dungey, J. W. 1958, *Cosmic Electrodynamics*, Cambridge University Press

Fontenla, J. M., Avrett, E. H., & Loeser, R. 1990, Energy balance in the solar transition region. I - Hydrostatic thermal models with ambipolar diffusion, *ApJ*, 355, 700–718

Giovanelli, R. G. 1982, Sunspot geometry and pressure balance, *Solar Phys.*, 80, 21–31

Giovanelli, R. G. & Jones, H. P. 1982, The three-dimensional structure of atmospheric magnetic fields in two active regions, *Solar Phys.*, 79, 267–278

Guhathakurta, M., Fisher, R. R., & Altrock, R. C. 1994, The Solar Cycle Variation of Coronal Temperature and Density During Cycle 21 - 22, *Adv. Space Res.*, 14, 49–52

Heyvaerts, J. & Priest, E. R. 1984, Coronal heating by reconnection in DC current systems - A theory based on Taylor's hypothesis, *A&A*, 137, 63–78

Hudson, H. S. 1991, Solar flares, microflares, nanoflares, and coronal heating, *Sol. Phys.*, 133, 357–369

Jarrett, A. H. & von Klüber, H. 1958, Interferometric Investigation of Emission Lines of the Solar Corona During the Total Solar Eclipse of 1958 October 12, *MNRAS*, 122, 223–238

Kaiser, R. & Salat, A. 1994, Surface current equilibria from a geometric point of view, *Physics of Plasmas*, 1, 281–295

Lin, H., Penn, M. J., & Tomczyk, S. 2000, A New Precise Measurement of the Coronal Magnetic Field Strength, *ApJ*, 541, L83–L86

Lin, J., Zhang, Z. D., Wang, Z., & Smartt, R. N. 1992, The morphological characteristics and cooling mechanisms of the post-flare loop system of April 28, 1980, *A&A*, 253, 557–560

Low, B. C. 1975, Nonisothermal magnetostatic equilibria in a uniform gravity field. I - Mathematical formulation, *ApJ*, 197, 251–255

Low, B. C. 1977, Evolving force-free magnetic fields. II - Stability of field configurations and the accompanying motion of the medium, *ApJ*, 217, 988–998

Low, B. C. 1980, On magnetostatic equilibrium in a stratified atmosphere, *Solar Phys.*, 65, 147–165

Low, B. C. 1985, Three-dimensional structures of magnetostatic atmospheres. I - Theory, *ApJ*, 293, 31–43

Low, B. C. 1991, Three-dimensional structures of magnetostatic atmospheres. III - A general formulation, *ApJ*, 370, 427–434

Low, B. C. 1992, Formation of electric-current sheets in the magnetostatic atmosphere, *A&A*, 253, 311–317

MacQueen, R. M., Eddy, J. A., Gosling, J. T., Hildner, E., Munro, R. H., Newkirk, G. A. J., Poland, A. I., & Ross, C. L. 1974, The Outer Solar Corona as Observed from Skylab: Preliminary Results, *ApJ*, 187, L85–L88

MacQueen, R. M., Sime, D. G., & Picat, J.-P. 1983, The Properties of Coronal Voids, *Solar Phys.*, 83, 103–114

Menzel, D. H. 1968, A Magnetohydrostatic Model of the Solar Corona., *AJ*, 73, S71–S72

Neukirch, T. 1997, Nonlinear self-consistent three-dimensional arcade-like solutions of the magnetohydrostatic equations., *A&A*, 325, 847–856

Newkirk, G. J., Dupree, A., & Schmahl, E. 1970, Magnetic Fields and the Structure of the Solar Corona II: Observations of the 12 November 1966 Solar Corona, *Solar Phys.*, 15, 15–39

November, L. J. & Koutchmy, S. 1996, White-Light Coronal Dark Threads and Density Fine Structure, *ApJ*, 466, 512–528

Parker, E. N. 1960, The Hydrodynamic Theory of Solar Corpuscular Radiation and Stellar Winds., *ApJ*, 132, 821–866

Parker, E. N. 1972, Topological Dissipation and the Small-Scale Fields in Turbulent Gases, *ApJ*, 174, 499–510

Parker, E. N. 1979, *Cosmical Magnetic Fields: Their Origin and Their Activity*, Clarendon Press, Oxford

Parker, E. N. 1987, Magnetic Reorientation and the Spontaneous Formation of Tangential Discontinuities in Deformed Magnetic Fields, *ApJ*, 318, 876–887

Petschek, H. E. & Thorne, R. M. 1967, The Existence of Intermediate Waves in Neutral Sheets, *ApJ*, 147, 1157–1163

Pneuman, G. W. & Kopp, R. A. 1978, Downflow in the supergranulation network and its implications for transition region models, *Solar Phys.*, 57, 49–64

Priest, E. R. 1972, A modification and criticism of Petschek's mechanism, *MNRAS*, 159, 389–402

Schatten, K. H., Wilcox, J. M., & Ness, N. F. 1969, A Model of Interplanetary and Coronal Magnetic Fields, *Solar Phys.*, 6, 442–455

Schmieder, B., Forbes, T. G., Malherbe, J. M., & Machado, M. E. 1987, Evidence for gentle chromospheric evaporation during the gradual phase of large solar flares, *ApJ*, 317, 956–963

Scudder, J. D. 1992, On the causes of temperature change in inhomogeneous low-density astrophysical plasmas, *ApJ*, 398, 299–318

Syrovatskii, S. I. 1981, Pinch Sheets and Reconnection in Astrophysics, *ARA&A*, 19, 163–229

Vainshtein, S. I. & Parker, E. N. 1986, Magnetic nonequilibrium and current sheet formation, *ApJ*, 304, 821–827

Van Ballegooijen, A. A. 1985, Electric currents in the solar corona and the existence of magnetostatic equilibrium, *ApJ*, 298, 421–430

Vernazza, J. E., Avrett, E. H., & Loeser, R. 1981, Structure of the Chromosphere. III. Models of the EUV Brightness Components of the Quiet Sun, *ApJS*, 45, 635–725

Wagner, W. J., Newkirk, G. J., & Schmidt, H. U. 1983, An Observation of Prominence Condensation out of a Coronal Void, *Solar Phys.*, 83, 115–119

Williams, L. L. & Mullan, D. J. 1996, Correlating Coronal Temperature and Gravitational Potential: A Test of the Nonthermal Boundary Hypothesis, *ApJ*, 457, L95–L98

Woo, R., Armstrong, J. W., Bird, M., & Patzold, M. 1995, Fine scale structure in coronal streamers, *ApJ*, 449, L91–L94

Woo, R. & Habbal, S. R. 1997, Finest Filamentary Structures of the Corona in the Slow and Fast Solar Wind, *ApJ*, 474, L139–L142

Zweibel, E. G. & Hundhausen, A. J. 1982, Magnetostatic Atmospheres: A Family of Isothermal Solutions, *Solar Phys.*, 76, 261–299